

Manipulation of band gap in 1*T*-$TiSe_2$ via rubidium deposition

Yi Ou(欧仪), Lei Chen(陈磊), Zi-Ming Xin(信子鸣), Yu-Jing Ren(任宇靖), Peng-Hao Yuan(袁鹏浩), Zheng-Guo Wang(王政国), Yu Zhu(朱玉), Jing-Zhi Chen(陈景芝), and Yan Zhang(张焱)
Citation: Chin. Phys. B, 2024, 33 (**8**): 087401. DOI: 10.1088/1674-1056/ad48f9

What follows is a list of articles you may be interested in

Surface doping manipulation of the insulating ground states in $Ta_2Pd_3Te_5$ and $Ta_2Ni_3Te_5$

Bei Jiang(江北), Jingyu Yao(姚静宇), Dayu Yan(闫大禹), Zhaopeng Guo(郭照芃), Gexing Qu(屈歌星), Xiutong Deng(邓修同), Yaobo Huang(黄耀波), Hong Ding(丁洪), Youguo Shi(石友国), Zhijun Wang(王志俊), and Tian Qian(钱天)
Chin. Phys. B, 2024, 33 (**6**): 067402. DOI: 10.1088/1674-1056/ad362e

Electronic structure and effective mass of pristine and Cl-doped $CsPbBr_3$

Zhiyuan Wei(魏志远), Yu-Hao Wei(魏愉昊), Shendong Xu(徐申东), Shuting Peng(彭舒婷), Makoto Hashimoto, Donghui Lu(路东辉), Xu Pan(潘旭), Min-Quan Kuang(匡泯泉), Zhengguo Xiao(肖正国), and Junfeng He(何俊峰)
Chin. Phys. B, 2024, 33 (**5**): 057403. DOI: 10.1088/1674-1056/ad3c31

Distinct behavior of electronic structure under uniaxial strain in $BaFe_2As_2$

Jiajun Li(李佳俊), Giao Ngoc Phan, Xingyu Wang(王兴玉), Fazhi Yang(杨发枝), Quanxin Hu(胡全欣), Ke Jia(贾可), Jin Zhao(赵金), Wenyao Liu(刘文尧), Renjie Zhang(张任杰), Youguo Shi(石友国), Shiliang Li(李世亮), Tian Qian(钱天), and Hong Ding(丁洪)
Chin. Phys. B, 2024, 33 (**1**): 017401. DOI: 10.1088/1674-1056/acd8af

Rubidium-induced phase transitions among metallic, band-insulating, Mott-insulating phases in 1*T*-TaS_2

Zhengguo Wang(王政国), Weiliang Yao(姚伟良), Yudi Wang(王宇迪), Ziming Xin(信子鸣), Tingting Han(韩婷婷), Lei Chen(陈磊), Yi Ou(欧仪), Yu Zhu(朱玉), Cong Cai(蔡淙), Yuan Li(李源), and Yan Zhang(张焱)
Chin. Phys. B, 2023, 32 (**10**): 107404. DOI: 10.1088/1674-1056/acec40

Measurement of electronic structure in van der Waals ferromagnet $Fe_{5-x}GeTe_2$

Kui Huang(黄逵), Zhenxian Li(李政贤), Deping Guo(郭的坪), Haifeng Yang(杨海峰), Yiwei Li(李一苇),Aiji Liang(梁爱基), Fan Wu(吴凡), Lixuan Xu(徐丽璇), Lexian Yang(杨乐仙), Wei Ji(季威),Yanfeng Guo(郭艳峰), Yulin Chen(陈宇林), and Zhongkai Liu(柳仲楷)
Chin. Phys. B, 2022, 31 (**5**): 057404. DOI: 10.1088/1674-1056/ac5c3c

---

RAPID COMMUNICATION

Manipulation of band gap in 1T-$TiSe_2$ via rubidium deposition

Yi Ou(欧仪), Lei Chen(陈磊), Zi-Ming Xin(信子鸣), Yu-Jing Ren(任宇靖), Peng-Hao Yuan(袁鹏浩), Zheng-Guo Wang(王政国), Yu Zhu(朱玉), Jing-Zhi Chen(陈景芝), and Yan Zhang(张焱)[†]

International Center for Quantum Materials, School of Physics, Peking University, Beijing 100871, *China*

(Received 8 March 2024; revised manuscript received 24 April 2024; accepted manuscript online 9 May 2024)

The 1T-$TiSe_2$ is a two-dimensional charge-density-wave (CDW) material that attracts great interest. A small band gap locates at the Fermi level separating the Ti d-bands and Se p-bands, which makes 1T-$TiSe_2$ a promising candidate for realizing excitonic condensation. Here, we studied the band gap in 1T-$TiSe_2$ using angle-resolved photoemission spectroscopy (ARPES). Instead of only focusing on the in-plane band dispersions, we obtained the detailed band dispersions of both conduction and valance bands along the out-of-plane direction. We found that the conduction and valance bands split into multiple sub-bands in the CDW state due to band folding. As a result, the band gap between the Ti d-bands and Se p-bands reduces to $\sim$ 25 meV and becomes a direct gap in the CDW state. More intriguingly, such band gap can be further reduced by the rubidium deposition. The band structure becomes semimetallic in the rubidium-doped sample. Meanwhile, exotic gapless behaviors were observed at the p–d band crossing. Our result characterized the band gap of 1T-$TiSe_2$ in three-dimensional Brillouin zone with unpreceded precision. It also suggests a closing of band gap or a potential band inversion in 1T-$TiSe_2$ driven by rubidium deposition.

Keywords: angle-resolved photoemission spectroscopy, metal–insulator transition, transition metal dichalcogenides

PACS: 74.25.Jb, 74.70.Xa, 79.60.–i **DOI:** 10.1088/1674-1056/ad48f9

1. Introduction

For semiconductors and semi-metals, band gap is a critical characteristic of electronic structure, which determines most physical properties of materials, such as transport properties, photoelectric properties, topological properties, etc.[1,2] Therefore, looking for a way to manipulate the band gap becomes an important direction of research for the application of semiconductors and semi-metals. Typically, the band gap can be regulated by modulating the crystal structure parameters through pressure or chemical substitution.[3–5] The change of structure parameters modulates the intra-band hopping and inter-band interactions, and thereby changes the band gap. Recently, in ultrathin and two-dimensional materials, it has been found that the electric field that applied perpendicular to the sample surface can also modulate the band gap of the material effectively through the Stark effect.[6–9] The vertical electric field changes the potential difference and the band mixing between the valence and conduction bands, which normally leads to a reduction of band gap in the two-dimensional semiconductors.

The 1T-$TiSe_2$ is a typical transition-metal-chalcogenide material. Charge-density-wave (CDW), superconductivity, and excitonic instability are all found in 1T-$TiSe_2$, making 1T-$TiSe_2$ one of the most studied systems in two-dimensional materials.[10–13] The low-energy band structure of 1T-$TiSe_2$ can be viewed as a three-bands system.[14,15] The Se p-orbitals contribute two hole-like bands at the Brillouin zone center (0,0) while the Ti d-orbitals contribute one electron-like band at the Brillouin zone boundary (0,π). Early band calculations suggest that 1T-$TiSe_2$ is a semi-metal with a negative band gap between the Se p-bands and Ti d-bands.[14] However, later angle-resolved photoemission spectroscopy (ARPES) studies show that the material is a semiconductor with an indirect band gap separating the Se p-bands and Ti d-bands.[16,17]

For a small gap semiconductor, excitonic instability is important. It has been proposed that the CDW transition of 1T-$TiSe_2$ is driven by an exciton condensation.[13,15,18,19] An excitonic insulating state has been proposed where the Bose–Einstein condensation (BEC) of excitons occurs.[20,21] Early ARPES studies on the in-plane band structure of 1T-$TiSe_2$ found an increment of band gap between the conduction band and valence band in the CDW state, which favors the excitonic condensation scenario.[15,18] However, recently, an ARPES study observed a strong modulation of band gap along the out-of-plane direction, suggesting that the CDW may be driven by an orbital-selective band hybridization.[17] 1T-$TiSe_2$ is a quasi-two-dimensional material. Thereby, its out-of-plane band dispersion is normally overlooked. Here, we characterized the out-of-plane band dispersion of 1T-$TiSe_2$ using synchrotron-based ARPES. We found that the band structure in the CDW state of 1T-$TiSe_2$ can be well explained considering a band folding of the $2 \times 2 \times 2$ CDW order along both in-plane and out-of-plane directions and a band hybridization between the Ti d-band and Se p-band. The band gap between the

[†]Corresponding author. E-mail: yzhang85@pku.edu.cn

© 2024 Chinese Physical Society and IOP Publishing Ltd

Ti d-band and Se p-band is reduced to be around 25 meV in the CDW state. More intriguingly, we found that such band gap can be further reduced by the electric field generated by the rubidium surface deposition. In the rubidium-doped sample, the band structure becomes semi-metallic and a gapless state was observed at the p–d band crossing. Our result explains how the bands reconstruct in the CDW state of $1T$-$TiSe_2$ in the three-dimensional Brillouin zone. It also suggests the existence of a band gap closing or a band inversion in rubidium-doped $1T$-$TiSe_2$.

2. Materials and methods

High-quality single crystals of $1T$-$TiSe_2$ were synthesized using chemical vapor transport (CVT) method. By mixing the appropriate ratio of Ti powder and Se pieces (2% excess) well, the compound was sealed in a quartz tube using iodine as the transport agent. The quartz tube was put in the two-zone furnace with thermal gradient between 560 °C and 640 °C for 336 h. ARPES data were taken at BL03U beamline of Shanghai Synchrotron Radiation Facility (SSRF) and also at Peking University using a helium discharging lamp. The overall energy resolution was ~ 12 meV and the angular resolution was $\sim 0.3°$. The crystals were cleaved *in-situ* and measured in vacuum with a base pressure better than 6×10^{-11} mbar. The alkali-metal deposition was performed *in situ* using a rubidium dispenser. For each deposition step, we only kept the rubidium evaporator at the working current for few tens of seconds to achieve a fine doping step, and then took ARPES spectra. The depositing time is defined as the total time of the rubidium deposition.

3. Results and discussion

We first characterized the band structure of $1T$-$TiSe_2$ above the CDW transition temperature. The Brillouin zone of $1T$-$TiSe_2$ is shown in Figs. 1(a) and 1(b). At the (0,0) point, we observed two valance bands (v_1 and v_2) [Fig. 1(c)]. They are constructed by the Se p-orbitals. The band tops of v_1 and v_2 show moderate k_z dispersions [Fig. 1(d)]. When moving from A to Γ, both v_1 and v_2 shift towards the Fermi energy (E_F). The band maximum of v_1 is at the Γ point, locating at ~ 45 meV below E_F. For the conduction band, one band (c_1) was observed near the L point [Fig. 1(e)]. It is constructed by the Ti d-orbitals. The k_z dispersion of c_1 is consistent with the band calculation.[14,17] The c_1 band is far away from E_F at M and thereby cannot be observed by ARPES. When the k_z moves from M to L, the c_1 band shifts towards E_F. If the sample temperature is high, electrons can be thermally excited to the states above E_F and thereby can be detected by ARPES. Our data taken at 235 K [Fig. 1(e)] clearly exhibit the c_1 band at the L point whose band bottom is at ~ 15 meV above E_F. Our data are consistent with previous ARPES studies, confirming that above the CDW transition temperature, the band structure of $1T$-$TiSe_2$ is characterized as a small gap semiconductor. The indirect band gap is around 60 meV. It is also worth to be noted that a broad feature was observed at high binding energy in Fig. 1(e). One explanation is that the broad feature reflects the band folding originating from the short-range CDW order above the CDW transition temperature. It has also been proposed that the broad feature is induced by the strong electron–exciton coupling effect in $1T$-$TiSe_2$.[22]

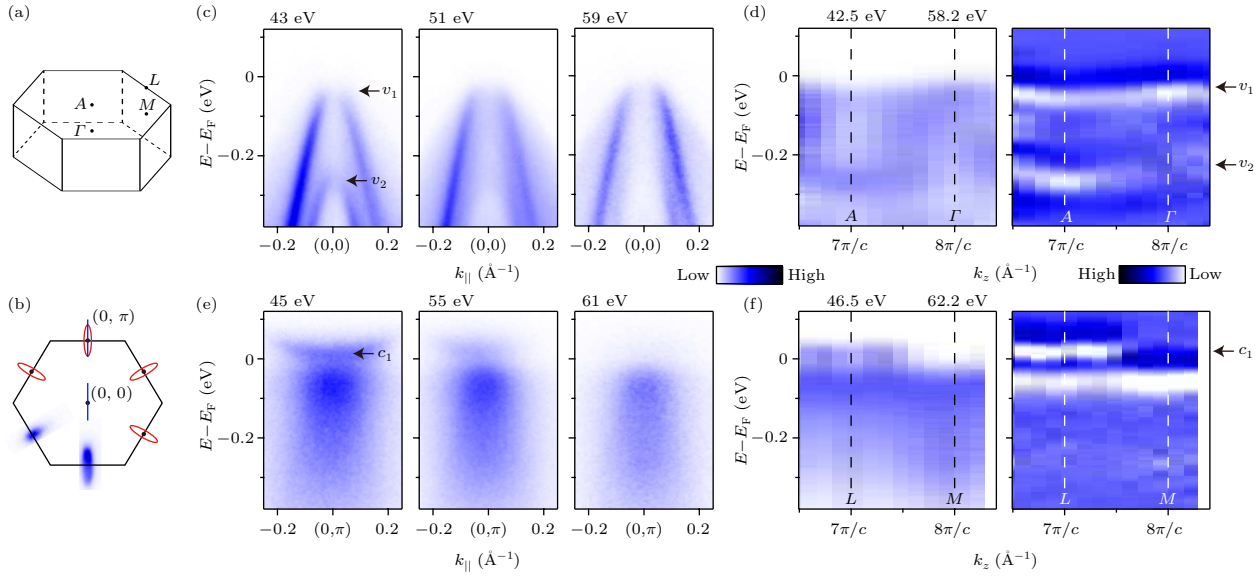


Fig. 1. The band structure of $1T$-$TiSe_2$ above the CDW transition temperature. (a) Schematic drawing of the three-dimensional Brillouin zone of $1T$-$TiSe_2$. (b) Fermi surface mapping of $1T$-$TiSe_2$ taken at 250 K using 21.2 eV photons. The two-dimensional Brillouin zone and the cut positions are illustrated. (c) Photon energy dependent cuts taken at the Brillouin zone center (0,0). (d) Energy–momentum cut (left panel) and its second derivative image (right panel) taken along the A–Γ direction. The energy distribution curves taken at different photon energies are merged into one image to better illustrate the k_z dispersions. (e) is the same as (c) but taken at the Brillouin zone boundary (0,π). (f) is the same as (d) but taken along the L–M direction. All the photon energy dependent data were taken at 235 K.

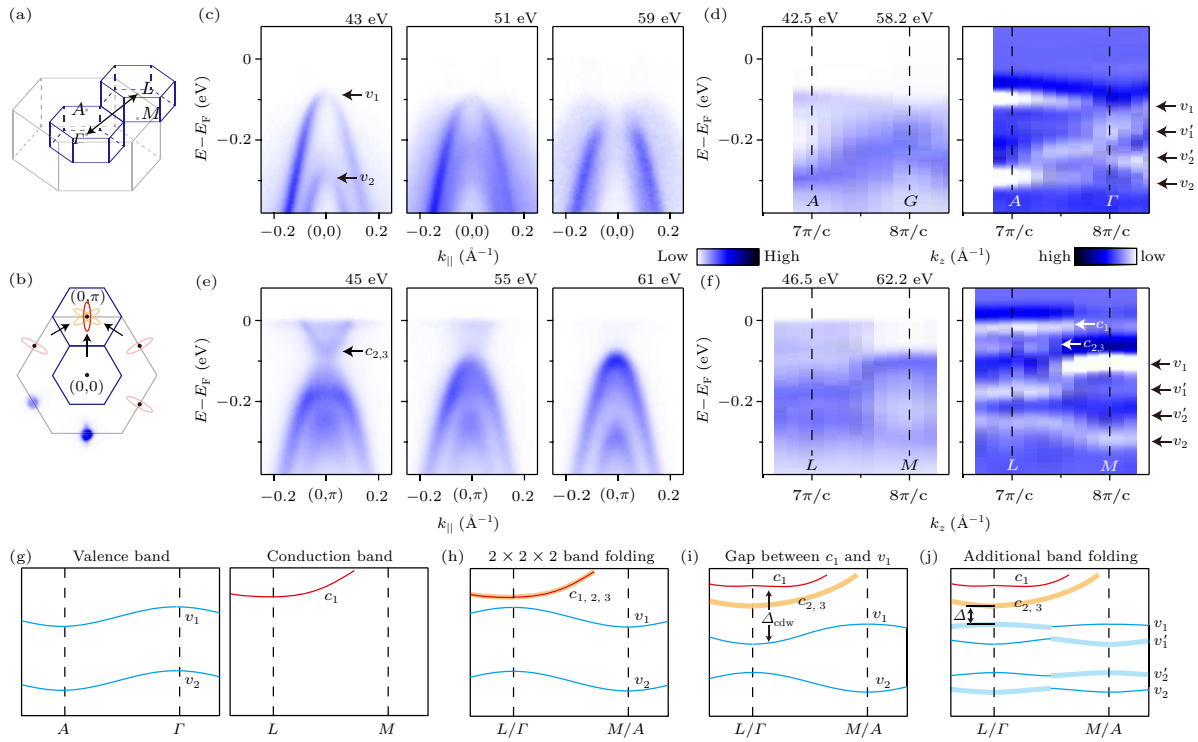


Fig. 2. The band structure of 1T-$TiSe_2$ below the CDW transition temperature. (a) Schematic drawing of the folded three-dimensional Brillouin zone of 1T-$TiSe_2$ in the CDW state. The folding vector is illustrated using a black arrow. (b) Fermi surface mapping of 1T-$TiSe_2$ taken at 11 K using 21.2 eV photons. The folding of Fermi pocket and the two-dimensional Brillouin zone are illustrated. (c) Photon energy dependent cuts taken at (0,0). (d) Energy–momentum cut (left panel) and its second derivative image (right panel) taken along the A–Γ direction. The energy distribution curves taken at different photon energies are merged into one image to better illustrate the k_z dispersions. (e) is the same as (c) but taken at the (0,π). (f) is the same as (d) but taken along the L–M direction. All the photon energy dependent data were taken at 15 K. (g) Schematic drawing of the band dispersions along the A–Γ and L–M directions above the CDW transition temperature. (h) Schematic drawing of the band dispersions along the L–M direction considering the $2 \times 2 \times 2$ band folding. (i) and (j) are the same as (h) but further considering the gap opening and additional band folding, respectively.

Figure 2 shows the photon energy dependent data taken below the CDW transition temperature. In the CDW state, the bands fold and the Brillouin zone reduces [Figs. 2(a) and 2(b)]. As shown in Figs. 2(c) and 2(d), in comparison with bands in the normal state, the valence bands are nearly unchanged at the A point, but reconstruct significantly at the Γ point. Four sub-bands (v_1, v_1', v_2, and v_2') could be resolved in the CDW state. At the zone boundary [Figs. 2(e) and 2(f)], the CDW order folds the valence bands to the (0,π) point. Therefore, the four sub-bands v_1, v_1', v_2, and v_2' could also be resolved in the k_z band dispersion taken along the L–M direction [Fig. 2(f)]. However, we note that the $2 \times 2 \times 2$ CDW vector of 1T-$TiSe_2$ has an out-of-plane component [Fig. 2(a)]. Instead of connecting Γ and M, the CDW vector connects Γ and L. As a result, in comparison to the main bands [Fig. 2(d)], the k_z dispersions of the folded valence bands reverse in the data taken along the L–M direction [Fig. 2(f)]. For the conduction bands, as shown in Fig. 2(b), the CDW order folds the two nearby electron bands to the (0,π) point. The conduction bands are thereby three-fold degenerated at the (0,π) point in the CDW state [Fig. 2(h)]. Considering a band hybridization between c_1 and v_1, the hybridization gap opens around the L/Γ point [Fig. 2(i)]. This explains the huge reconstruction of v_1 observed at the Γ point [Figs. 2(c) and 2(d)]. It also explains the energy splitting of c_1 and $c_{2,3}$ observed in Fig. 2(f). Furthermore, considering the doubling of unit cell along the c-axis in the CDW state of 1T-$TiSe_2$, there is an additional band folding between L/Γ and M/A [Fig. 2(j)]. This explains the observation of four sub-bands (v_1, v_1', v_2, and v_2') in Figs. 2(d) and 2(f). It is expected that the additional band folding should also be applied for the c_1 and $c_{2,3}$ bands. However, the photoemission intensity of the folded bands may be too weak to be observed in our data due to the matrix element effect. Overall, six sub-bands were observed in the CDW states of 1T-$TiSe_2$, which can be explained well by the band folding of the $2 \times 2 \times 2$ CDW order and the hybridization gap opening between c_1 and v_1.

It is intriguing to note that the band gap separating the Ti d-bands and Se p-bands becomes a direct gap (Δ) in the CDW state [Fig. 2(j)]. The gap is around 25 meV between the $c_{2,3}$ and v_1 bands. It has been shown that the alkali-metal deposition could tune the band gap of a two-dimensional semiconductor by generating a vertical electric field at the sample surface.[6,23,24] We then performed the surface deposition of rubidium on 1T-$TiSe_2$. Figure 3 shows the doping dependence of the $c_{2,3}$ and v_1 bands. Instead of a rigid-band shift, the $c_{2,3}$ and v_1 bands respond to the rubidium deposition differently. While both the $c_{2,3}$ and v_1 bands shift to higher binding energy, the band shift of $c_{2,3}$ is roughly three times larger than that of v_1. As a result, the band gap between $c_{2,3}$ and v_1 decreases to nearly zero in the 170 s doped sample.

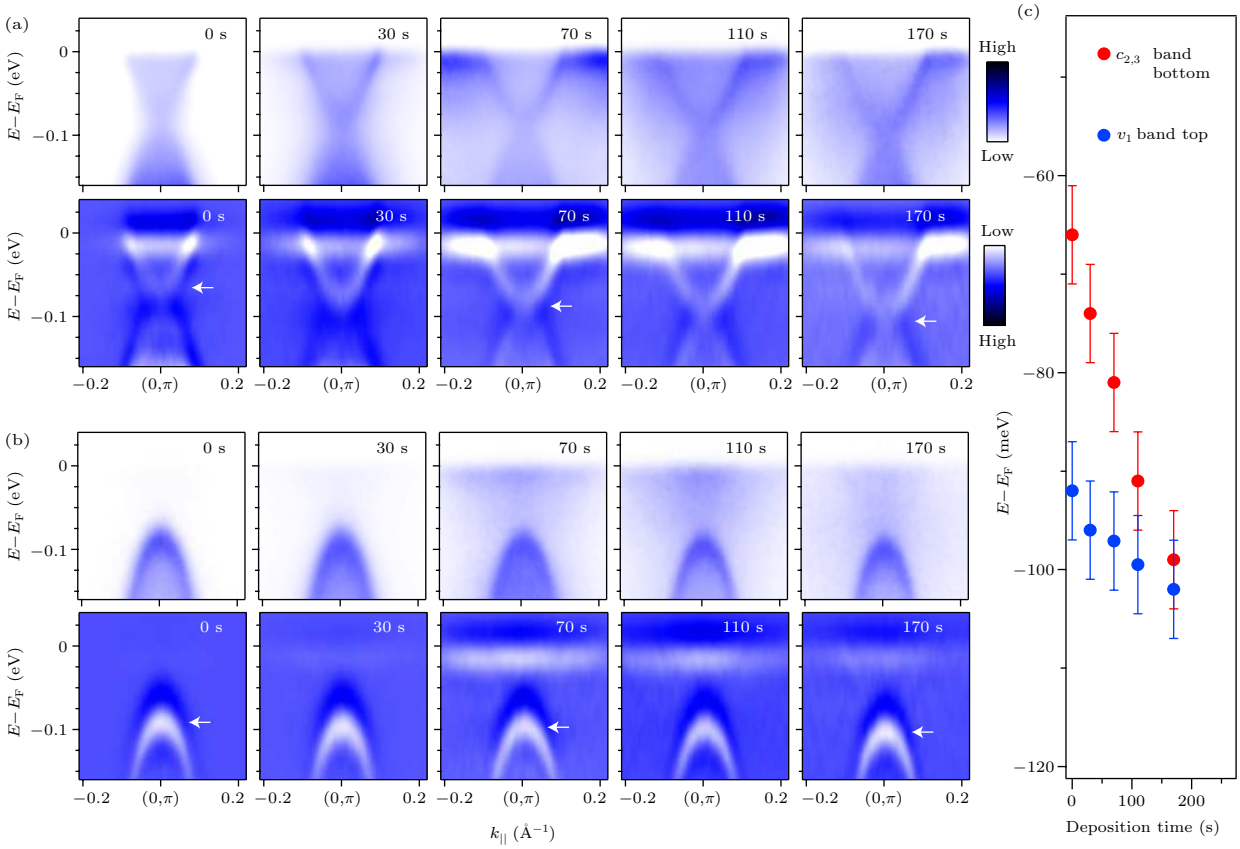


Fig. 3. The doping dependence of the band gap in rubidium-doped 1T-TiSe$_2$. (a) Doping dependence of the raw images (upper panels) and the second derivative images (lower panels) of the energy–momentum cuts taken at (0, π). The data were taken at 51 eV photon energy to illustrate the energy shift of the $c_{2,3}$ band bottom. (b) is the same as (a) but taken at the 61 eV photon energy to illustrate the energy shit of the v_1 band top. (c) Doping dependence of the $c_{2,3}$ band bottom and the v_1 band top. The band positions were determined based on the second derivative images and the EDC peak positions. The error bars were estimated based on the peak width in the second derivative images and the EDCs.

When the band gap of a semiconductor decreases to zero or negative, the band crossing between the valance band and the conduction band occurs. If no inter-band interaction is considered, the two bands would cross each other without any gap opening as shown in Fig. 4(a). However, if the inter-band interaction is turned on, the hybridization gap opens between the two bands and the band crossing is avoided [Fig. 4(b)]. However, none of these behaviors was observed in rubidium-doped 1T-TiSe$_2$. In the pristine sample, the 25 meV band gap was clearly resolved in the energy–momentum cut [Fig. 4(c)]. The band gap could be further confirmed by the EDCs where the two separated peaks were resolved around −80 meV [Fig. 4(d)]. In contrast, in the 110 s doped sample, the energy–momentum cut shows a clearly gapless behavior [Fig. 4(e)]. Consistently, the two EDC peaks merged into one peak whose photoemission intensity reaches the maximum at the band crossing [Fig. 4(f)]. The observed spectra indicate a gapless behavior between $c_{2,3}$ and v_1, which excludes the interacting scenario [Fig. 4(b)]. If the inter-band interaction is prohibited, then one would expect a simple band crossing between $c_{2,3}$ and v_1 when the band gap becomes negative [Fig. 4(a)]. Figure 4(g) shows the energy–momentum cut taken in a heavily-doped sample. Due to the electron doping of rubidium, the Fermi crossings of the conduction band are now two times larger than that in the 110 s doped sample. However, contrary to the simple band crossing scenario [Fig. 4(a)], the band meeting point remains unchanged at around −100 meV. Its momentum is located at the (0, π) point.

We first discuss the three-dimensionality of the band structure of 1T-TiSe$_2$. Our data provide a detailed characterization of the k_z band dispersion of 1T-TiSe$_2$ above and below the CDW transition temperature. We found that the k_z band dispersion and the out-of-plane component of the CDW vector cannot be overlooked. We confirmed that a band hybridization occurs between the c_1 and v_1 bands in the CDW state. Such band hybridization is strongly k_z dependent. It is only significant at the L and Γ points where the band minima of c_1 and band maximum of v_1 locate. The momentum vector that connects the L and Γ points matches the $2\times2\times2$ CDW vector. Therefore, our results suggest that the band hybridization between c_1 and v_1 bands plays an important role in driving the CDW in 1T-TiSe$_2$. Such hybridization could be referred to the exciton formation on the c_1 and v_1 bands[15,18,21] or to an orbital redistribution due to the change of lattice parameters.[17,25,26]

Similar to other two-dimensional materials, the band gap of 1T-TiSe$_2$ can be manipulated by the alkali-metal deposition. Since the band gap of 1T-TiSe$_2$ is relatively

small, a semiconductor to semi-metal transition is induced in rubidium-doped 1T-$TiSe_2$. It is intriguing that no hybridization gap is detected with our energy resolution when the c_2/c_3 and v_1 bands touch with each other. On one hand, our results may suggest that the electron–hole interactions in 1T-$TiSe_2$ are strongly band selective. While strong band hybridization exists between c_1 and v_1, the inter-band interaction between $c_{2,3}$ and v_1 is prohibited. On the other hand, the ARPES data taken in the heavily-doped sample seems to suggest that the momentum of the gapless state is pinned to the $(0,\pi)$ point. This may indicate that the band hybridization between c_2/c_3 and v_1 is strongly momentum dependent. While the band hybridization is prohibited at the $(0,\pi)$ point, the hybridization gap opens at other momenta. Nevertheless, the emergence of a gapless state in rubidium-doped 1T-$TiSe_2$ is unexpected, which requires further experimental and theoretical studies.

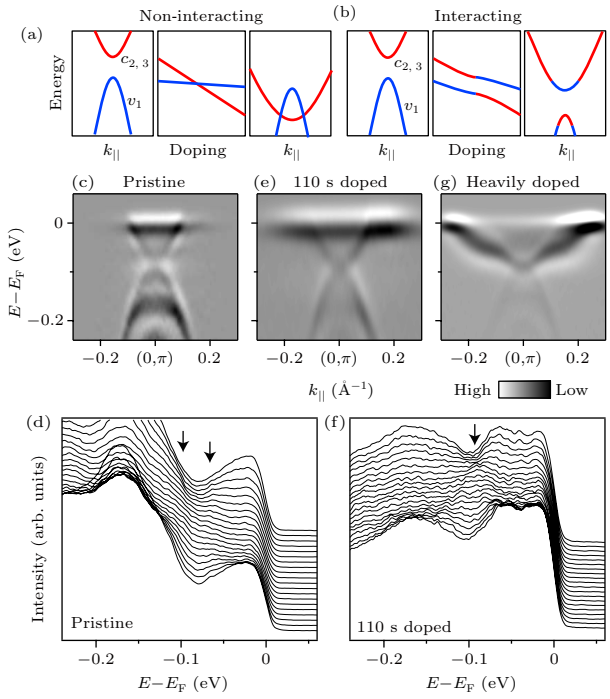


Fig. 4. The gapless electronic state observed in rubidium-doped 1T-$TiSe_2$. (a) Schematic drawing of the band inversion in a non-interacting scenario. (b) is the same as (a) but considering the interaction between $c_{2,3}$ and v_1. (c) The second derivative images of the energy–momentum cuts taken at the $(0,\pi)$ point in the pristine samples using 52 eV photon energy. (d) The EDCs extracted from the data in panel (c). (e) is the same as (c) but taken in the 110 s doped sample using 53 eV photon energy. (f) The EDCs extracted from the data in panel (e). (f) The second derivative images of the energy–momentum cuts at the $(0,\pi)$ point taken in the heavily-doped sample using 21.2 eV photon energy.

4. Conclusion and perspectives

In summary, we characterized the band structure of 1T-$TiSe_2$ in three-dimensional Brillouin zone using synchrotron-based ARPES. Our data highlight the importance of k_z band dispersion and the out-of-plane component of the CDW order in 1T-$TiSe_2$. To construct an effective theoretical model that describes the physics of 1T-$TiSe_2$, the hopping and interactions along the out-of-plane direction should be considered. More intriguingly, we observed a gap closing behavior in rubidium-doped 1T-$TiSe_2$. The result not only demonstrates that the alkali-metal deposition is an effective way to manipulate the band gap of two-dimensional semiconductors, but also suggests the existence of a gapless state in the gap-tuned 1T-$TiSe_2$. The origin of the gapless state requires further understanding. Band calculations and symmetry analysis need be conducted on all the related bands in the CDW state of 1T-$TiSe_2$. It is also intriguing to measure the transport properties of 1T-$TiSe_2$ using a gate-tuning device. With the unique small-gap semiconducting band structure, 1T-$TiSe_2$ serves as an ideal platform to study the excitonic phenomena, CDW, and topological properties of two-dimensional materials.

Acknowledgments

Project supported by the National Key Research and Development Program of China (Grant Nos. 2022YFA1403502 and 2018YFA0305602) and the National Natural Science Foundation of China (Grant No. 11888101). The work at SSRF is supported by ME2 project under contract No. 11227901 from the National Natural Science Foundation of China.

References

[1] Capasso F 1987 *Science* **235** 172
[2] Chaves A, Azadani J G, Alsalman H, *et al.* 2020 *npj 2D Mater. Appl.* **4** 29
[3] Coduri M, Shiell T B, Strobel T A, *et al.* 2020 *Mater. Adv.* **1** 2840
[4] Zeng M, Liu J, Zhou L, *et al.* 2020 *Nat. Mater.* **19** 528
[5] Choi W S, Chisholm M F and Singh D J 2012 *Nat. Commun.* **3** 689
[6] Ishigami M, Sau J D, Aloni S, Cohen M L and Zettl A 2005 *Phys. Rev. Lett.* **94** 056804
[7] Ramasubramaniam A, Naveh D and Towe E 2011 *Phys. Rev. B* **84** 205325
[8] Kang M, Kim B, Ryu S H, *et al.* 2017 *Nano Lett.* **17** 1610
[9] Kim J, Baik S S, Ryu S H, *et al.* 2015 *Science* **349** 723
[10] Wilson J A and Yoffe A D 1969 *Adv. Phys.* **18** 193
[11] Di Salvo F J, Moncton D E and Waszczak J V 1976 *Phys. Rev. B* **14** 4321
[12] Morosan E, Zandbergen H W, Dennis B S, *et al.* 2006 *Nat. Phys.* **2** 544
[13] Kogar A, Rak M S, Vig S, *et al.* 2017 *Science* **358** 1314
[14] Fang C M, Groot D R A and Haas C 1997 *Phys. Rev. B* **56** 4455
[15] Money C, Cercellier H, Clerc F, *et al.* 2009 *Phys. Rev. B* **79** 045116
[16] Zhao J F, Ou H W, Wu G, *et al.* 2007 *Phys. Rev. Lett.* **99** 146401
[17] Watson M D, Clark O J, Mazzola F, *et al.* 2019 *Phys. Rev. Lett.* **122** 076404
[18] Cercellier H, Monney C, Clerc F, *et al.* 2007 *Phys. Rev. Lett.* **99** 146403
[19] Pillo T, Hayoz J, Berger H, Levy F, Schlapbach L and Aebi P 2000 *Phys. Rev. B* **61** 16213
[20] Kohn W 1967 *Phys. Rev. Lett.* **19** 439
[21] Bronold F X and Fehske H 2006 *Phys. Rev. B* **74** 165107
[22] Zhu L, Zhao W M, Jia Z Y, *et al.* 2023 *Chin. Phys. Lett.* **40** 057101
[23] Chen L, Han T T, Cai C, *et al.* 2020 *Phys. Rev. B* **102** 161116
[24] Riley J M, Meevasana W, Bawden L, *et al.* 2015 *Nat. Nanotech.* **10** 1043
[25] Rossnagel K, Kipp L, Skibowski M, *et al.* 2002 *Phys. Rev. B* **65** 235101
[26] Wegner A, Zhao J, Li J, *et al.* 2020 *Phys. Rev. B* **101** 195145